Section A-Research paper

Bimetallic nanoparticles incorporated with Graphene oxide as an excellent absorbent in the removal of Methylene Blue

K.Gayathri*,P.Andal, [†],S.Tamijselvy

Vels institute of science technology and advanced studies

Department - Chemistry, School -Basic Sciences, Pallavarm,

Kancheepuram DistrictChennai-600117, Tamil Nadu, India.

Mobile Number:9884146295,Email:andalprithu.sbs@velsuniv.ac.in

Abstract:

This article describes the preparation, characterization and Kinetics of bimetallic alloy nanoparticles of GO-Ni-Cu NPs. The main objective of this review is to quantitatively, and comprehensively describe the synthesis of bimetallic nanoparticles, and characterization. The kinetic studies were carried out as a function of different variables like pH, and temperature on rate of decolorization. The activation energy in presence of Go- Ni(II) and Go-Cu(II) is lower than in its Go-Ni-Cu. The reaction to be $[H^+]$ because the first order in both $[MB^+]$ and reductant. The rate was found to increase linearly with temperature. The rate of decolorization decreased after the addition of Ni(II), but increased after the addition of Cu(II). The decrease in the activation energy(Ea) in presence of these transition metal ions confirms their catalytic effects (metal activation). Cu–Ni BNP implant to the graphene oxide surface and it increases the catalytic activity and also dispersion capacity.

Keywords: *Nickel, Copper, Nanoparticles, Methylene Blue, Graphene oxide, Activation energy*

Introduction

Bimetallic nanoparticles (BMNP) have excelled monometallic nanocrystals owing to their improved electronic, optical, and catalytic performances. BMNP often enhanced the selectivity of metal-catalyzed reactions. In addition, altering the metal composition opens up new possibilities for modifying the characteristics of BMNP beyond the conventional manipulation of size and shape, it can Alloy,random,core-shelland cluster – in- cluster. BNP can lead to catalysts with improved turnover rates and selectivities, but many synthetic protocols, such as impregnation or precipitation, typically form particles of non-uniform size and composition.The electrical effect and also the synergistic is high because of their catalytic performance, BMNPs have recently attracted a lot of attention [1-2]. Investigated as well are the effects of aggregation on the magneto-resistance of thick Ni-based films [3] and the magnetic characteristics of Ni nanoparticles produced via hydrogen reduction [4]. Solid oxide fuel cells frequently use powdered nickel and copper as active anode material. Compared to the majority of noble metal salts, which are typically util-utilized catalysts, transition metal salts like Cu and Ni are more affordable and easily accessible. Nickel Copper has an efficient catalyst than MNP nickel [5-6]. Numerous techniques for creating bimetallic and alloyed Ni-Cu particles have been suggested in order to enhance the characteristics of pure Ni and Cu powders. Ni-Cu-Al [7], Ni-Cu/Al2O3 [8], and Ni-Cu alloys [9] have all been produced by reducing a mixture of nickel and copper compounds in the presence of hydrogen. Bimetallic Ni-Cu colloids are produced by the evaporation of a Ni-Cu alloy and co-condensation with organic solvents [10].Mo¨rke et al. [11] On SnO2, Ni-Cu alloy particles with a nominal ratio of 60:40 were created, and their magnetic properties were assessed using ferromagnetic resonance. Using the polyol process technique for producing metal powders with uniform particle size and shape in controlled circumstances, has also been use to synthesize of s bimetallic and alloy powders including Ni or Cu [12].

[†] *Address of Co-Author 1: Department of chemistry, School of Basic sciences,*

Vels University, Pallavaram, Chennai - 600117

In an aqueous buffered (sodium acetate-acetic acid) media, the kinetics of alpha hydroxy acid oxidation by peroxomonosulfate (PMS) catalysed by Ni(II) ions and CO(II) have been investigated. In [PMS] and [Ni(II)], the reaction follows first order, but in [H+], it follows inverse first order. Both HSO5- and SO52- are thought to be the active forms of the oxidant based on the effect of pH on the rate [12-16]. In the present study, an attempt is made to investigate the decolorization kinetics of methylene blue with sodium sulphite in aqueous media by UV-Visible spectrophotometry. The effect of various parameters such as initial pH, initial concentration of sulphite, MB+ and transition metal ions concentration was studied.

Experimental

The structure and also the properties of Graphene oxide depend upon, the method used for synthesis and also the degree of oxidation. In Graphene oxide, graphene sheets are maximumly decorated with epoxide and also hydroxyl functional groups. Commonly used method for synthesis namely Modified Hummer's method. Graphite flakes of 5 grams and Sodium nitrate of 2.5 grams were mixed in 115ML of Sulphuric acid taken in a 1000ML beaker. The mixer stirred for 30 minutes and the temperature should be maintained 0^o -5^o C. After 30 minutes of stirring 20 grams of potassium permanganate were added gradually. The mixed solution was stirred for 2 hours with 0^o-5^o C. After 2 hours of stirring, the temperature changed to 35^oC, it should be stirred again for two hours. The distilled water of 230ML was added dropwise after the temperature changed to 98^oC for 15 minutes. After 15 minutes 700ML of distilled water and 50ML of Hydrogen peroxide were added. Then allow to yellowish-brown color precipitate. It should be washed several times and centrifuged

then filtered with 10% of Hydrochloric acid, then several washes with distilled water. After filtration, it should be dry under a vacuum at room temperature.

A stock solution of Na_2SO_3 and MB^+ was prepared using the required aofunt in distilled water. A Na_2SO_4 solution was addedthe to reaction mixthe ture in order to maintain the ionic strength of the solution. The effect of pH was also studied by adjustment of pH of the reaction mixture prior to decolorization with NaOH or HCl and measured by a pH meter (JENWAY 3505 pH meter). The effect of temperature was studied and also its controlled using horizontal thermostated shaker (SM 101 by Surgafriend Medicals). The absorbance of the reaction mixture at different reaction times was recorded by measuring the absorption intensity at 661nm max of MB^+ λ using Genesys 10 UV-VIS Scanning Spectrophotometer. The reaction mixtures were allowed to undergo complete reaction as evident from the constancy of repeated measurements of absorbance ($A\infty$) at 661 nm. The concentration at any time t(Ct) was obtained from the difference in the absorbance at time t(At) and at infinity ($A\infty$) .

The same quantity and the procedure used for BNP and MNP catalysts viz., Cu, Ni NPs were also prepared. The reduction of Ni^{2+}, Cu^{2+} to Ni Cu NPs was noticed through the change of color. Using Raman, XRD, UV, and Biological analysis BNP particles are characterized.

Result & discussions

Excellent catalytic, thermal, and chemical characteristics can be found in graphene supported BNP. Between them, there are Vander Waals interactions and "-" stacking. These two elements cause permanent agglomerations, which reduce surface area and conductivity. The type of the metallic salt appears to have the greatest influence on the reduction process, followed by time and temperature. The reduction from the carbonates is still fairly challenging. The lengthening of time does not offset the impact of temperature. To synthesise

homogeneous mono/bimetallic nanoparticle catalysts, one needs an appropriate template to stabilize/encapsulate the metal nanoparticles. In the synthesis of homogeneous metal nanoparticles for use as the catalyst, it has been demonstrated that the identification of the template/stabilizing agent is a more challenging process.

It is also learned from the earlier studies that stabilization/encapsulation of bimetallic/monometallic nanoparticles using a single template has shown an excellent catalytic activity due to the co-operative/synergetic effect of more than one metal nanoparticles. Similarly, although the reduction of organic dyes, heavy metal ion, and anti-bacterial activity are already studied with other existing catalysts but also far, there is no report available for effective reduction of the said substrate using a heterogeneous catalyst that contains more than one metal nanoparticle as a catalyst. It is in this background, the present study deals with the synthesis of two different methods of graphene oxide supported BNP and MNP particles catalysts viz., Ni/Cu, and Ni Graphene oxide is a common stabilizing agent and NiNO3, and CuSO4 as a metal precursor for Ni NPs, CuNPs, metal nanoparticles through simplified procedures. The obtained two different methods of mono and bimetallic nanoparticle catalysts were characterized by Raman and XRD analyses. The comparative catalytic efficiency of two different types of mono and bimetallic nanoparticles catalysts were examined by conducting the reduction of organic dyes, heavy metal ion keeping under identical pseudo-second-order conditions in the presence of Na_2SO_3 and formic acid.

D band at 1354 $^{cm-1}$ and G band at 1549 $^{cm-1}$ the obtained spectra represents the presence of graphene oxide.[17]

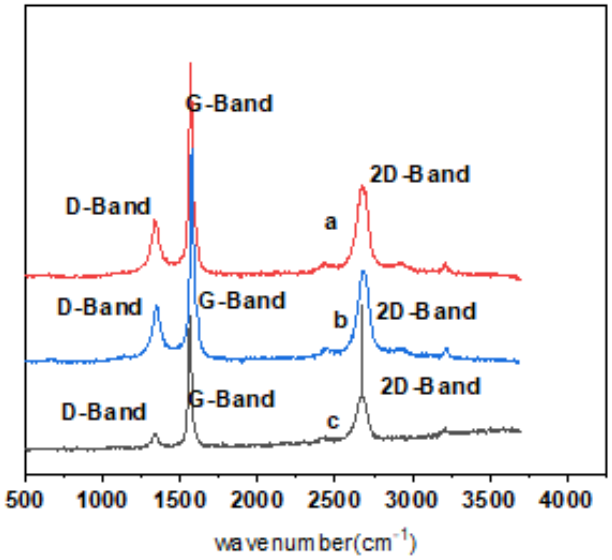

Raman spectra of (a)GO-Ni-Cu (b)GO-Cu (c) GO-Ni NPs

Raman peaks for graphene in copper (CuGO) and nickel (NiGO) are typical peaks with graphitic material at 1577 cm-1 and 2695 cm-1, respectively. The D band and the presence of monocrystalline domain sizes are assigned to the CuGO's extra peak at 1346 cm1.

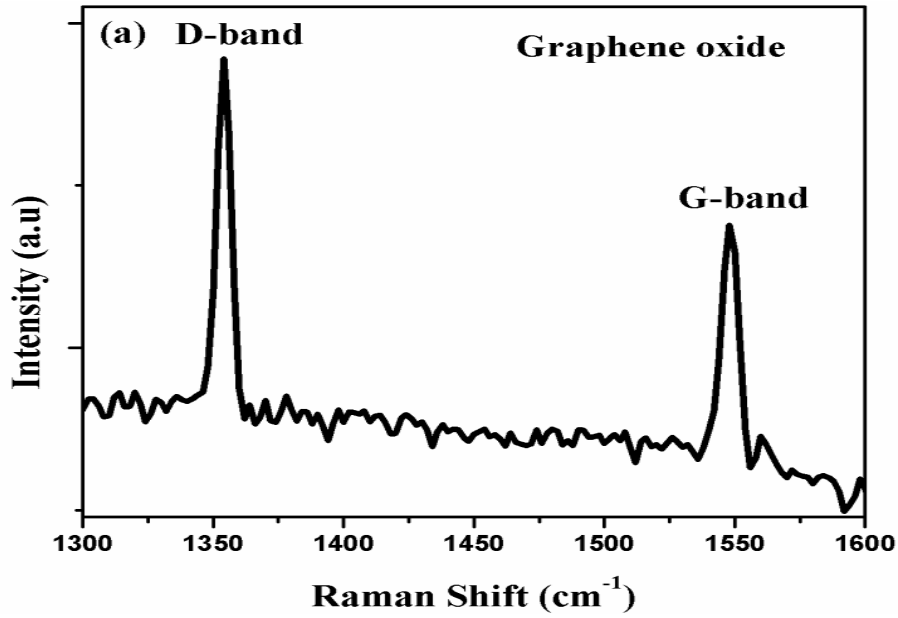

According to the formula La(nm) = (2.4 1010)4(ID/IG)1, the average crystallite size of the graphene on the copper foam was discovered to be 42.5 nm (SD = 8.4), averaged over 307

spectra. La stands for average crystallite size, is the wavelength used for laser excitation, and ID/IG is the proportion of D to G band intensities. An ID/IG frequency histogram for CuGO can be seen in the ESI. Since NiGO lacks a D-band, it is possible that the carbon compound produced is more crystalline. The several mechanisms involved in copper-mediated carbon development are most likely to blame for this. The sp2 framework is formed when carbon combines after adhering to the surface of copper. This surface-related mechanism makes it more prone to faults and bends in the metal template.

Although flat metal surfaces frequently use copper as the metal of choice for controlled graphene development, these substrates typically have a high degree of polish. The underlying 3-D copper catalyst monoliths formed in situ prior to carbon growth presumably have poor crystallinity and surface roughness, which contribute to the creation of severely defective graphene/graphitic material.

The X-ray diffractometer is used to check the successful manufacture of rGO, and the results can be used to describe changes in the interlayer spacing of GO and consequently, their reduction. The C (002) diffraction peak at 12.2° no longer occurs in the XRD pattern of GO. On rGO's XRD patterns, a broad diffraction peak can be seen at 24.4°. The smaller interlayer spacing brought on by the removal of oxygenated groups from the GO surface can be utilized to explain this outcome, proving that rGO was successfully prepared.

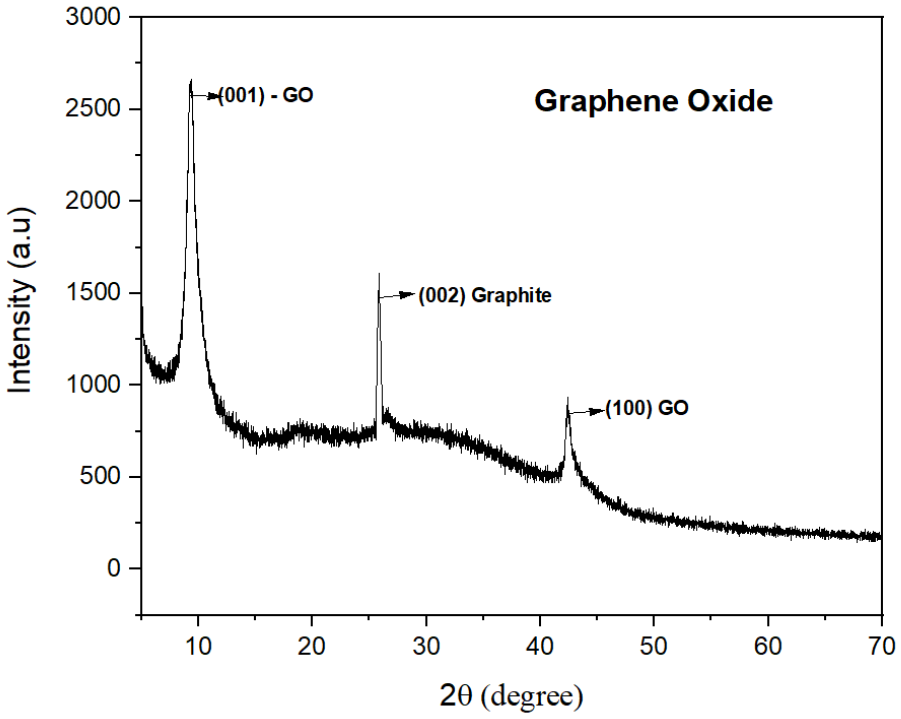

The GO supported bimetallic Ni-Cu alloy NPs ,XRD to determine the crystalline nature 2θ values between 20 to 80 ºC.

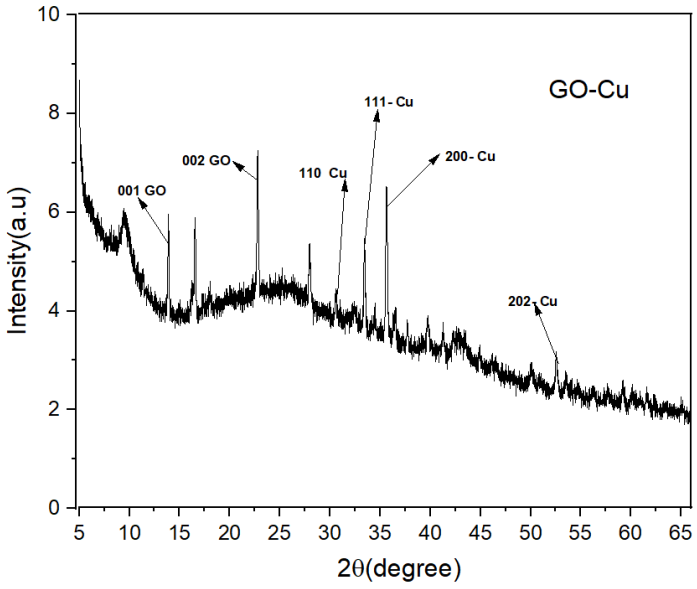

Figure 2 depicts the XRD patterns of GO, Ni Cu, and Go/Ni-Cu; GO is represented by two distinct diffraction peaks at around 10.05° and 42.3°. G showed diffraction peaks at roughly 26° and 43.5°, proving that GO was completely transformed to G. The Sigma-Aldrich nickel nanoparticles had NiO (JCPDS card number 87-712) as an impu

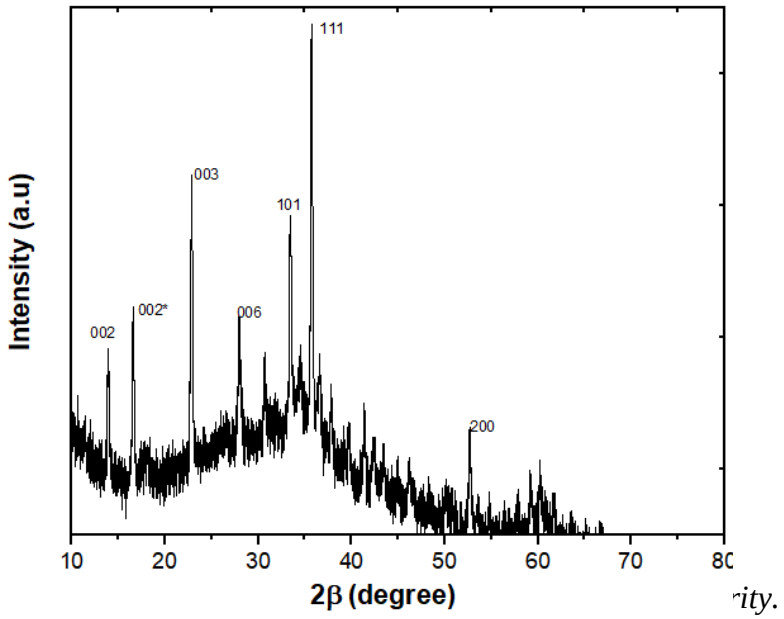

rity.

Fig.2. XRD Patterns of GO-Ni-Cu

The peak associated with LCO NPs was slightly displaced to a lower angle, as seen in the inset of Fig. 2, which demonstrated that La was loaded on the surface of CuO material. The distinctive peaks for crystalline bimetallic Ni-Cu NPs were depicted in Fig. 3. Ni-Cu NPs' characteristic 2 values correspond to the 002, 002, 003, 006,, 101, 111, and 200 planes at 20.01o, 36.02o, 38.1o, 44.2o, 64.4o, and 77.3o.*

The Debye-Scherer equation was used to determine the crystal sizes of the LCO and CuO NPs.: $D = \frac{K\lambda}{\beta cos\theta}$

where D is the catalyst's crystal size, K is an indivisible constant, is the X-ray wavelength, b is the diffraction peak's full width at half-maximum (FWHM), and q is the

diffraction angle We deduced from this equation that the LCO NPs' crystalline size was 35.72.

Inorganic synthesis, polymer science, petrochemical engineering, the pharmaceutical industry, and food analysis all use FTIR spectroscopy.

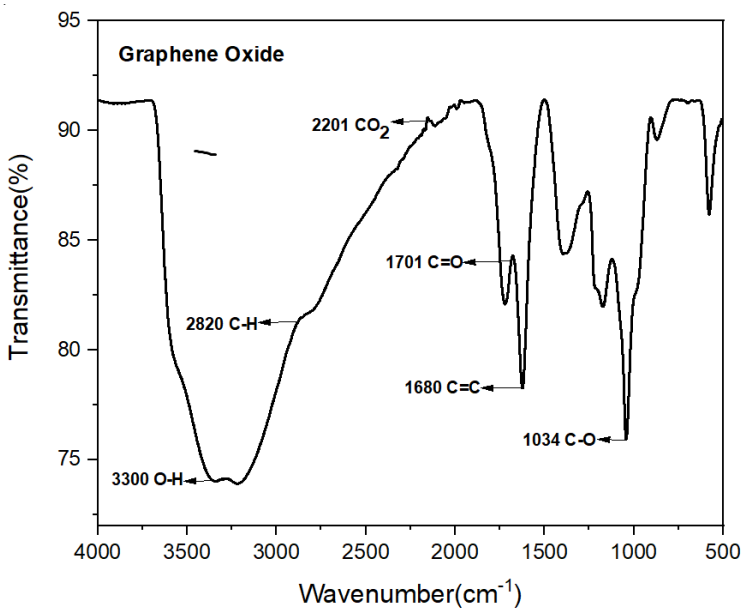

Due to hydroxyl stretching vibrations in COOH and/or intercalated water, the FTIR spectra of GO exhibits vibrational bands at about 3300 cm—1. Alkoxy C—O stretching vibrations are responsible for the bands at 1034 cm—1 and the strong band at 1680 cm—1, respectively.

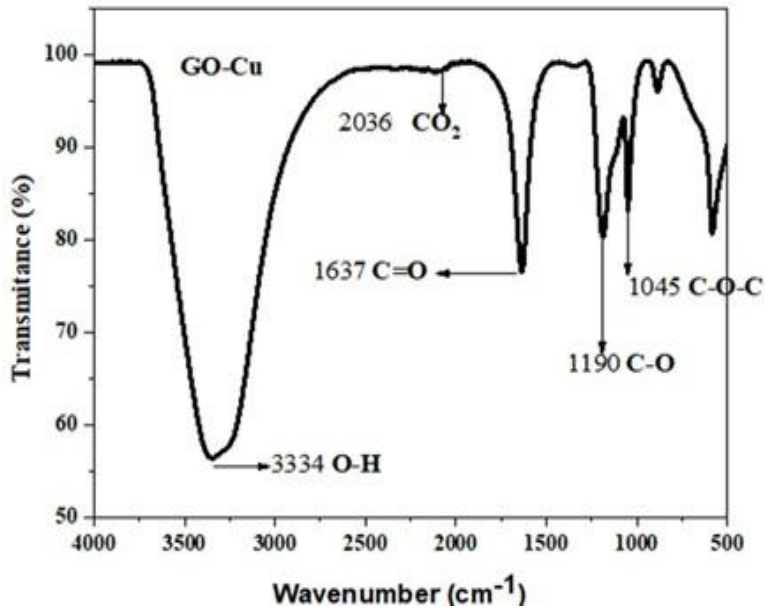

In our study IR spectrum of isolated solid graphene oxide and Copper products were compared against each other to determine any similarities or difference in the stretching frequencies. In the IR spectra GO has a strong and O-H stretch vibration band at 3334 cm^{-1}, C=O stretch at band at 1637cm^{-1}, C-O stretch at 1190cm^{-1}, C-O-C stretch band at 1045cm^{-1}.

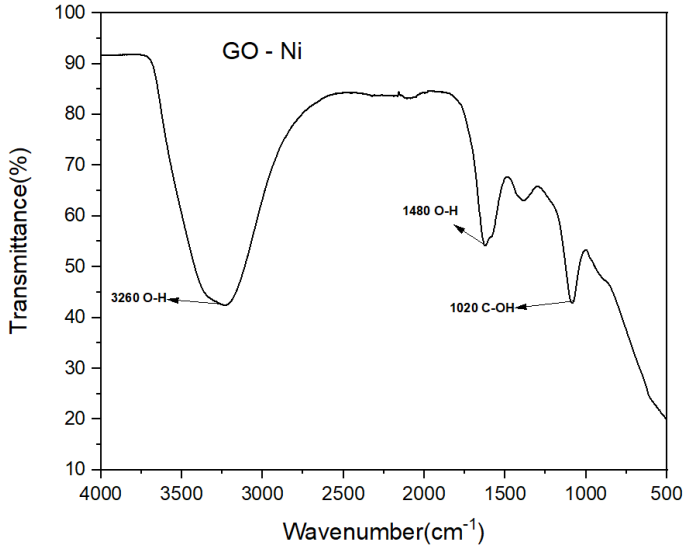

In the IR spectra GO has a strong and O-H stretch vibration band at 3260 cm^{-1}, O-H stretch band at 1480cm^{-1}, C-OH stretch at 1020cm^{-1}

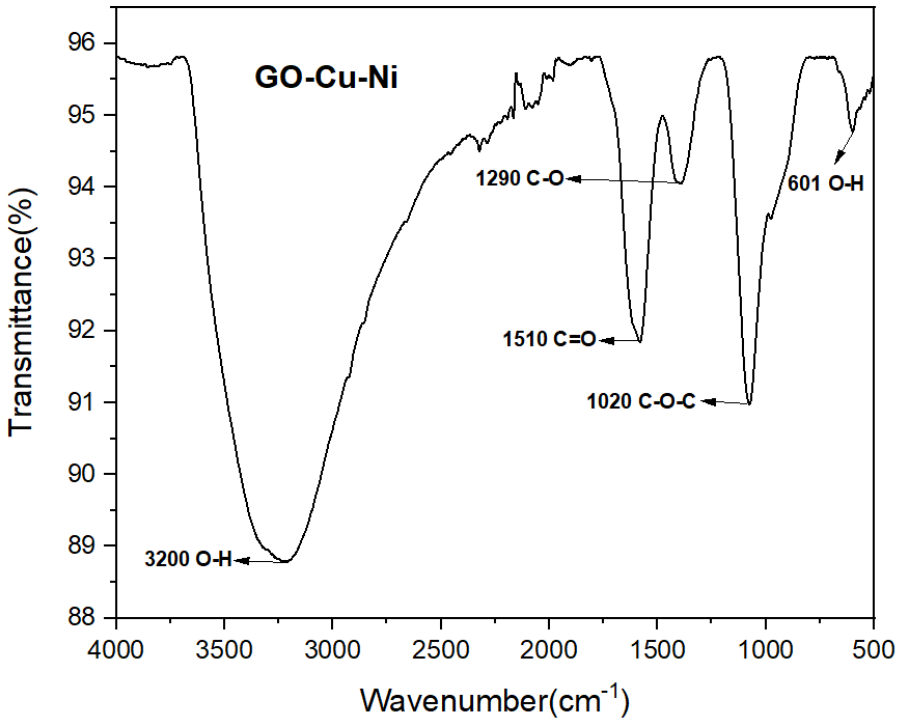

In our study IR spectrum of isolated solid graphene oxide and Copper-Nickel products were compared against each other to determine any similarities or difference in the stretching frequencies. In the IR spectra GO has a strong and O-H stretching vibration band at 3200 cm^{-1}, C=O stretching band at 1510cm^{-1}, C-O stretching at 1290cm^{-1}, C-O-C stretching band at 1020cm^{-1}.

*The UV-Visible absorption spectrum method is used to examine the electrical characteristics of graphene oxide/Ni-Cu. The GoNPs absorb the visible light in the range of (235-245) nm because the oscillation energy of their surface electrons (Plasmon) is in resonance with this wavelength. By taking note of the UV-visible absorption spectra, the GoNPs can be located. Two signals are visible in Go/Ni-UV-visible Cu's absorption spectra between 650 and 750 nm. The n - * transition is represented by the absorption signal at (300-400) nm, whereas the - * transition is represented by the signal at (650-750) nm. The characteristics of Go/Ni-Cu are these electrical qualities. he SPR signal of GoNPs at xx nm is*

visible in the UV-visible absorption spectra of Go/Ni-Cu, which supports the synthesis of GoNPs. The GoNPs with NiCu Nano conjugates exhibit two significant absorption signals at (300-400)nm and (650-750)nm in addition to the SPR peak at (235-245) nm. It demonstrates that beta carotene molecules have been conjugated to GoNPs.

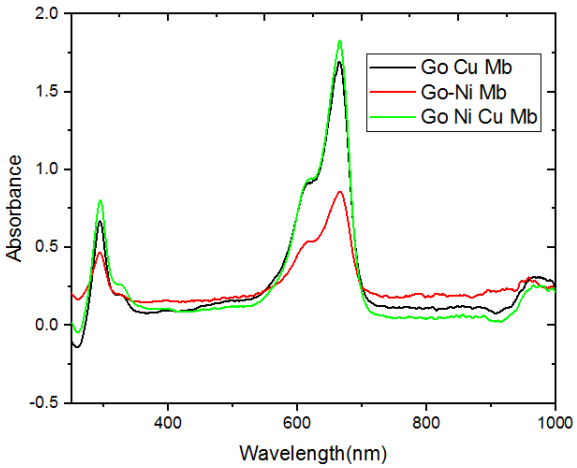

Fig.3. UV Spectra of GO Cu Mb,GO Ni Mb,Go Ni Mb

Additionally, the antibacterial properties of graphene oxide supported mono and bimetallic nanoparticle catalysts. Gram-positive Enterococcus faecalis and Gram-negative Pseudomonas aeruginosa were chosen for antibacterial testing because they are frequently found in infections that affect patients. By calculating anti-bacterial ratios based on the number of bacterial colonies incubated with various dosages of GO-supported mono and bimetallic nanoparticles at 37 °C after a contact time of 1 h, as shown in Figure. 4-5, the comparative anti-bacterial property of GO-Ni-Cu, nanoparticles was investigated.

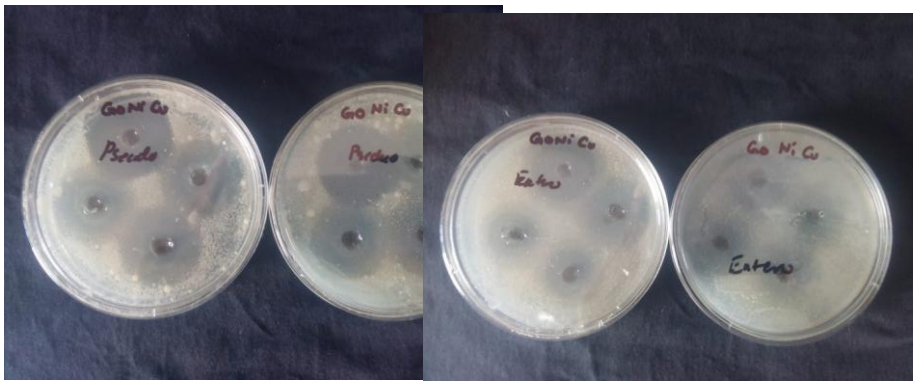

Fig.4. Antibacterial activity of pseudomonas aeruginosa

Fig.5.Antibacterial activity of Enterococcus faecalis

Table.1

Sample	*Species*	*Zone of inhibition (in mm)*			
		15mg	*20mg*	*25mg*	*Control(Streptomycin-10mg)*
	Enterococcus faecalis	*8*	*8*	*8*	*18*
		8	*8*	*8*	*18*
		8	*8*	*8*	*18*
	Pseudomonas aeruginosa	*18*	*24*	*26*	*30*
		16	*23*	*26*	*30*
		17	*24*	*26*	*30*

According to these findings, GO-supported bimetallic nanoparticles are superior than monometallic nanoparticles at killing Gram-negative pseudomonas aeruginosa and Gram-positive Enterococcus faecalis bacteria.

Kinetic study for the reduction of Methylene blue using Graphene Oxide supported Cu-Ni NPs catalyst

Cu-Ni NPs, a superior catalyst, was used and investigated under pseudo-first order reaction conditions in order to determine the impact of [Na2SO3], [substrate], and [Catalyst] on the reduction of organic dyes. The UV-vis spectrophotometer was used as normal to measure the product's absorbance against time with a declining trend at 670 nm in order to track the kinetics of the dyes reduction reaction. According to the reported rate constants, the reduction of organic dyes substrate has been greatly influenced by [Na2SO3], [substrate], and [catalyst]..

Effect of starting stage of concentration of MB^+

Figure 6 depicts the relationship between the rate of MB+ depolarization by Na2SO3 and the initial MB+ concentration (10–40 mg/dm3) under the same conditions. It can be seen that the decolorization of MB+ starts out very quickly and slows down as the reaction develops. Na2SO3 almost fully decolorizes MB+ at low concentrations, as seen by the absorbance data that was collected alongside the reaction time. According to the temporal profiles of MB+, depolarization significantly decreases as MB concentration rises.

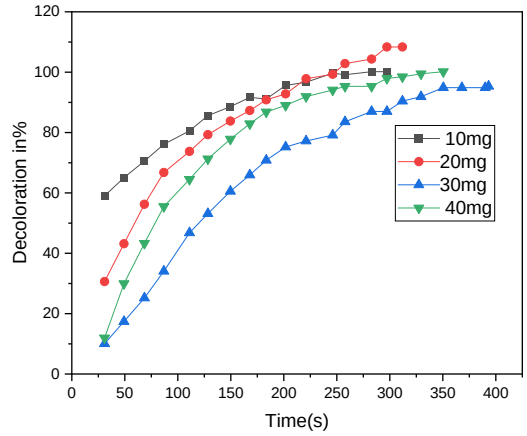

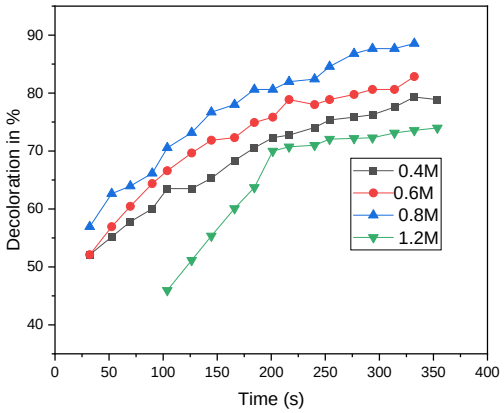

Fig.6. Effect of initial concentration of MB^+ ***Fig.7. Effect of initial concentration of SO_3^{2-}***

Effect of initial concentration of SO_3^{2-}

Na_2SO_3 decolonization of MB^+ was investigated using initial concentration of Na_2SO_3 from 0.4 to 1.2 mol/dm^3, the results are shown in ***Figure 7.*** *It was observed that the decolourization efficiency increases from 69.6% to 80.9% as a consequence of increasing Na_2SO_3 concentration from 0.4 to 1.2 mol/dm^3. This is due to increasing reductive power of the sulphite.*

Kinetic study

Due to the various reduced forms of MB+, it was challenging to examine the reductive decolorization of MB+ by sulphite. Simple reaction kinetics presented difficulties in representing the process. A power law equation is utilized to calculate the kinetics rate of decolorization.: $\frac{-d[A]}{dt} = k[SO_3^{2-}]^c[A]^d$----------*(1)*

Where c and d are the pseudo orders of reaction with respect to MB+ to SO32-, respectively, and k is the removal rate constant, [A] is the MB+ concentration. With the discovered rate constant (k_{obs}), the rate equation can be expressed as follows:

$$\frac{-d[A]}{dt} = k[A]^d \text{----------(2)}$$

Where,

$$k_{obs} = k[SO_3^{2-}]^C \text{----------(3)}$$

For a zero-order reaction, the above equation after integration becomes: $A_t = k_o t$

additionally, for a first-order reaction, the above equation after integration becomes:

$$ln(A_t) = ln(A_o) - k_1 t \text{----------(4)}$$

in which, Ao is the initial MB^+ concentration and A_t concentration at reaction time t.

The absorbance-time data plot of the above reaction orders was carried out to determine the rate constant, k_{obs} and excellent order for the reaction manner. The zero- and first- -order kinetics rate constants for the decolorization of MB^+ with SO_3^{2-} have been acquired from the plots, and the consequences had been shown in shown in Table 2. It was noticed that the correlation coefficients for the three models are non identical. The first order kinetics indicates highest correlation (R_2 >0.9) than zero -order kinetics (R_2 <0.9). It is able to therefore be concluded that the decolorization of MB^+ with SO_3^{2-} suits the first-order reaction kinetics of the type:

TABLE .2

Rates of the reaction in [MB^+] and [SO_3^{2-}]

S.No	***[SO_3^{2-}]moldm^{-3}***	***Zero order***		***First order***	
		k_0 x10^{-3}	***R^2***	***k_1 x10^{-3}***	***R^2***
1.	*0.4*	*1.6*	*0.567*	*8.0*	*0.960*
2.	*0.6*	*1.8*	*0.546*	*8.6*	*0.975*
3.	*0.8*	*2.4*	*0.553*	*11.1*	*0.972*
4.	*1.2*	*3.0*	*0.478*	*12.8*	*0.968*

S.No	$[MB^+]$mg/L	Zero order		First order	
		$k_0 x10^{-3}$	R^2	$k_1 x10^{-3}$	R^2
1.	10	3.6	0.462	1.67	0.959
2.	20	3.6	0.654	1.48	0.969
3.	30	3.8	0.764	1.28	0.989
4.	40	4.2	0.810	1.40	0.980

Effect of pH

In sight of the reality that pH of dye solution is a leading parameter on the decolorization progress, the experiments were accomplished to discover the top of the optimal pH of reaction combination for decolorization of MB^+. The inspected pH range become from 1-8, which changed into adjusted by means of the usage of assigned amounts of base(NaOH) or acid(HCl) solutions. It became found that the decolorization of MB^+ become considerably prompted by the solution's pH values, and the elevated decolorization rate (k_{obs}) become executed at pH 1.45. Those observations are in exact settlement with published consequences [18-22]

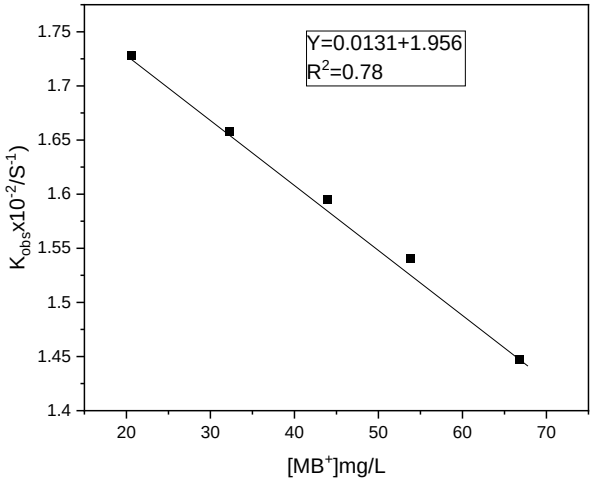

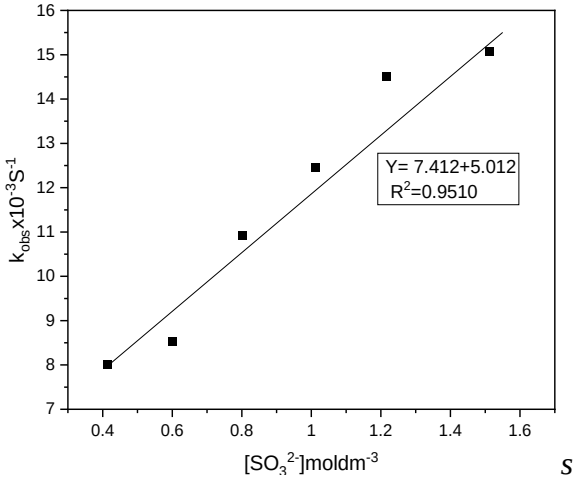

Fig.8.First-order dependence on the initial concentration of MB^+ for its reaction with

Fig.9.First-order dependence on the initial concentration of SO_3^{2-} for its reaction with

S

1.0 mol/dm^3 sulphite at pH 8-9 and 30°C. 20 mg/dm^3 sulphite at pH 8-9 and 30°C.

Effect of temperature

The impact of temperature on decolorization of methylene blue in the presence and absence of transition metal ions catalyst become carried out in the range of 293-313 K. The results in Figure 7 display that the decolorization performance of methylene blue gradually increased with increase in the temperature. The increase in temperature might also cause o increasing reduction rate of methylene blue. The activation parameters associated with the decolorization of methylene blue are calculated from the plot lnk_{obs} versus of 1/T (Figure 7), which offers the value of activation energy (Ea) , according to the Arrhenius equation.

$$lnk_{obs} = \frac{-Ea}{RT} + lnA \text{----------(5)}$$

The values of $\Delta H^{\#}$ and $\Delta S^{\#}$ can be calculated from the plot of the Eyring equation as follows :

$$lnk_{obs}/T = \left(ln\frac{k_B}{h} + \frac{\Delta S^{\#}}{R}\right) - \frac{\Delta H^{\#}}{RT} \text{----------(6)}$$

$$M^{n+} + Na_2SO_3 \xrightarrow{[O]} SO_3^{-\blacksquare} + M^{(n+1)+} + Na_2O \text{----------(7)}$$

Sulphite anion radical

$$SO_3^{-\cdot} + O_2 \rightarrow O_3^-SOO^{\blacksquare} \text{----------(8)}$$

Peroxymonosulphate anion radical

$$O_3^-SOO^{\blacksquare} + Na_2SO_3 \rightarrow Na_2SO_4 + SO_4^{-\blacksquare} \text{----------(9)}$$

Sulfate anion radical

$$SO_4^{-\blacksquare} + H_2O \rightarrow HO^{\blacksquare} + H^+ + SO_4^{2-} \text{----------(10)}$$

Where, k_B is the Boltzmann's constant (1.381×10^{-23} J K^{-1}); h is the Plank's constant (6.626×10^{-34} J.s), where ln k_B /h = 23.76 .The rate constants and activation energies in the range of temperature studied (20-40°C) are listed in Table 3 . The activation energy in presence of Go- Ni(II) and Go-Cu(II) is lower than in its Go-Ni-Cu(Table 3). The decrease in the activation energy (Ea) in presence of these transition metal ions confirms their catalytic effects (metal activation).

TABLE .3

Rate constants and activation parameters for interaction of MB^+ and SO_3^{2-} in the presence of catalyst.

S.No	***T(ºC)***	***k_{obs} x10^{-2}/s^{-1}***			***E_a/kJmol^{-1}***		
		GO-Ni-Cu	***GO-Ni***	***GO-Cu***	***GO-Ni-Cu***	***GO-Ni***	***GO-Cu***
1.	*20*	*0.84*	*2.09*	*2.01*	*38.01*	*37.39*	*33.28*
2.	*30*	*1.72*	*4.50*	*3.11*			
3.	*40*	*2.09*	*6.11*	*4.29*			

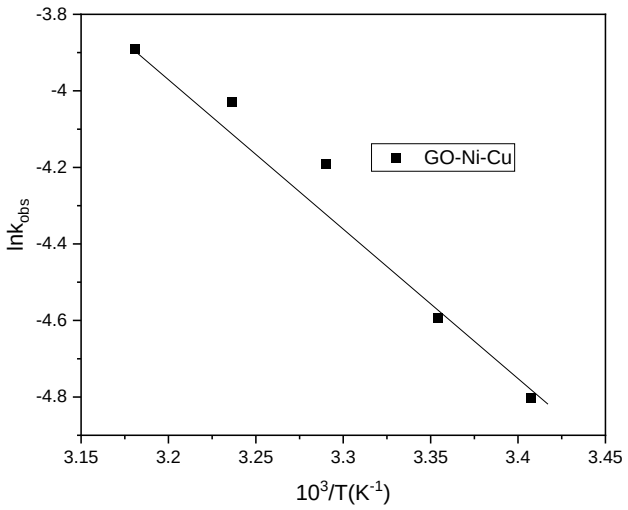

Fig.10 Arrhenius plot for the reaction of MB^+ with Na_2SO_3 in the presence GO-Ni-Cu

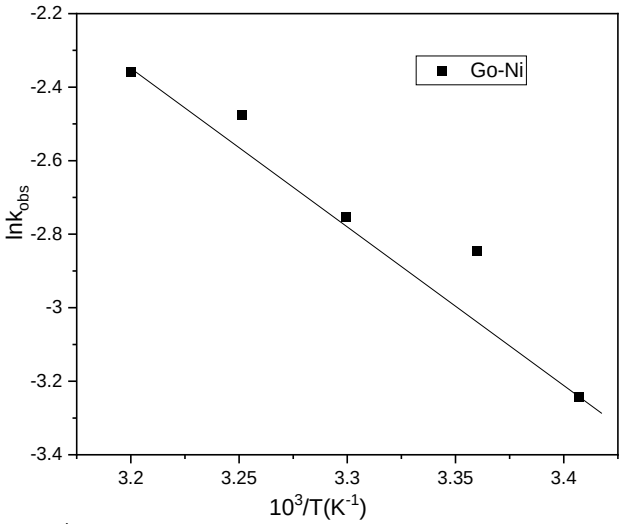

Fig.11 Arrhenius plot for the reaction of MB^+ with Na_2 SO_3 in the presence GO-Ni

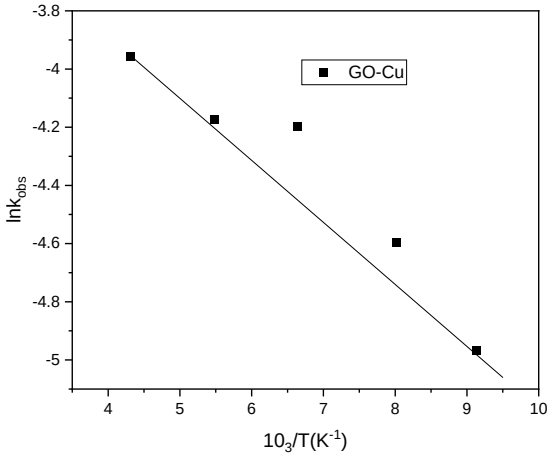

Fig.12 Arrhenius plot for the reaction of MB^+

with Na_2SO_3 in the presence GO-Cu

Reaction mechanism

Primarily, based on the above experimental findings and observations, the reaction mechanism has been counseled utilizing the redox redox properties of Na_2SO_3. It has additionally been referred to that redox reactions of many oxyanions are strongly acid dependent. Under the prevailing experimental conditions, it's miles reasonable to postulate that SO_3^{2-} is protonated in a quick step to give HSO^{3-} which then reacts with MB+ in a gradual step to present the products. Therefore, taking recourse to the experimental statistics data, the following mechanistic steps have been postulated for the reaction:

$$SO_3^{2-} + H^+ \overset{K1}{\leftrightarrow} HSO_3^- \text{----------(11)}$$

$$MB^+ + HSO_3^- \overset{k2}{\rightarrow} Products\text{-------(12)}$$

$$MB^+ SO_3^{2-} \overset{k3}{\rightarrow} Products\text{----------(13)}$$

$$Rate = k_2[MB^+][HSO_3^-] + k_3[MB^+][SO_3^{2-}]\text{----------(14)}$$

$$HSO_3^- = K_1[H^+][SO_3^{2-}]\text{----------(15)}$$

Substitute eqn(5) in eqn(4) we get

$$Rate = k_2K_1[MB^+][SO_3^{2-}][H^+] + k_3[MB^+][SO_3^{2-}]\text{-------(16)}$$

Therefore, the rate is expressed in terms of

$$Rate = (k_3 + k_2 K_1[H^+])[MB^+][SO_3^{2-}]\text{----------}(17)$$

where K_1 is the protonation constant, and k_2 and k_3 are the pseudo second order rate constants for the protonation and deprotonation of MB^+. Equation (22) shows acid dependence on the rate of decolorization of methylene blue with sodium sulphite and is similar to equation (12) with k_3 ='a'=1.32×10^{-2} dm^3 mol^{-1} s^{-1} and k_2 K_1 ='b'=0.595 dm^6 mol^{-2} s^{-1}.

Conclusion:

According to the results, newly discovered graphene oxide supported bimetallic nanoparticle catalysts can be more effective at oxidizing, reducing, and removing significant organic pollutants from the environment. They are also excellent physiologically active compounds. We looked into a number of variables, including MB dye concentration, adsorbent dosage, and contact time. It was discovered that the initial pH of the MB solution is crucial, with basic circumstances favoring MB adsorption. GO-Ni-Cu exhibits good adsorbent capabilities for cationic MB dye, with removal efficiency up to 98%, based on the removal rate of MB. Overall, it can be said that MB concentration and adsorbent dosage affect the adsorption rate. Kinetic analysis is used to examine how the cationic dye methylene blue loses color by becoming a reduced form of MB+ (colorless). Temperature, pH, and reactant concentration all affect how quickly color is removed. Regarding MB+ and SO32, the decolorization of MB+ is pseudo first order. After adding Cu(II), the decolorization in an acidic medium increases with temperature; however, adding Ni(II) causes a decrease in the decolorization.

Reference

1. *S. K. Bhargava, J. M. Booth, S. Agrawal, P. Coloe and G. Kar, Langmuir, 2005, 21, 5949-5956.*
2. *J. D. S. Newman and G. J. Blanchard, Langmuir 2006, 22, 5882-5887.*
3. *T. Ould Ely, C. Amiens, B. Chaudret, E. Snoeck, M. Verelst, Chem. Mater. 11 (1999) 536–539.*
4. *B. Morten, M. Prudenziati, F. Sirotti, G. de Cicco, L. Olumekor, J. Mater. Sci.: Mater. Electron. 1 (1990) 118–122.*
5. *Y. Li, J. Chen, L. Chang, Y. Qin, J. Catal. 178 (1998) 76–83.*
6. *F.M. Bautista, J.M. Campelo, A. Garcı´a, R. Guarden˜o, D. Luna, J.M. Marinas, J. Mol. Catal. A: Chem. 104 (1996) 229–235.*
7. *S.K. Shaikhutdinov, L.B. Avdeeva, O.V. Goncharova, D.I. Kochubey, B.N. Novgorodov, L.M. Plyasova, Appl. Catal. A: General 126 (1995) 125–139.*
8. *H. Noller, W.M. Lin, J. Catal. 85 (1984) 25–30.*
9. *R.G. Samel'yan, E.S. Abovyan, S.G. Agbalyan, N.N. Manukyan, M.S. Sakanyan, Soviet Powder Metall. Met. Ceram. 30 (1991) 606.*
10. *G.T. Cardenas, R.C. Oliva, Mater. Res. Bull. 33 (11) (1998) 1599–1608.*
11. *W. Morke, T. Bieruta, J. Jarsetz, C. Go¨rsmann, U. Schubert, Colloids Surf. A: Physicochem. Eng. Aspects 115 (1996) 303–309.*
12. *M. Figlarz, C. Ducamp-Sanguesa, F. Fie´vet, J.-P. Lagier , Metal Powder Industries Federation, Vol. 1, 1992.*
13. *P. Andal, M. Murugavelu, S. Shailaja, M. S. Ramachandran, Oxidation of Lactic acid Int. J.*

Chem. Kinet. 2009, 41, 449–454.

14. M. Murugavelu, P. Andal, S. Shailaja, M. S. Ramachandran, J. Mol. Catal. A: Chem. 2009, 306, 1-5.

15. G.Ragu Kumar , P. Andal, C. Lavanya,M. Murugavelu and M. S. Ramachandran J. Mol. Catal. A: Chem. 2014.

16. C. Lavanya, P. Andal, M. Murugavelu and M. S. Ramachandran Indian. J. Chem. 2015, 54A, 333-344.

17. Michael K. Tynan, David W. Johnson , Ben P. Dobson and Karl S. Coleman 2016, 8, 13303-13310

18. Fan HJ, Huang ST, Chung WH, Jan JL, Lin WY, et al. (2009) J Hazard Mater 171: 1032-1044.

19. . Abo-Farha SA (2010) Researcher 2: 1-20.

20. . Behnajady MA, Modirshahla N, Ghanbary F (2007) J Hazard Mater 148: 98-102.

21. . Sun JH, Sun SP, Wang GL, Qiao LP (2007) Dyes and Pigments 74: 647-652.

22. Malik PK, Sk S (2003) Sep Purif Technol 31: 241-250.